iMRI

Investigative Magnetic Resonance Imaging

Correspondence to:
Yoon-Chul Kim, Ph.D.
Clinical Research Institute,
Sungkyunkwan University School
of Medicine, Samsung Medical
Center, 81 Irwon-ro Gangnam-gu,
Seoul 06351, Korea.
Tel. +82-2-2148-7140
Fax. +82-2-3410-2559
E-mail: yoonckim@skku.edu,
yoonckim1@gmail.com

Advanced Methods in Dynamic Contrast Enhanced Arterial Phase Imaging of the Liver

Yoon-Chul Kim

Clinical Research Institute, Samsung Medical Center, Sungkyunkwan University School of Medicine, Seoul, Korea

Dynamic contrast enhanced (DCE) magnetic resonance (MR) imaging plays an important role in non-invasive detection and characterization of primary and metastatic lesions in the liver. Recently, efforts have been made to improve spatial and temporal resolution of DCE liver MRI for arterial phase imaging. Review of recent publications related to arterial phase imaging of the liver indicates that there exist primarily two approaches: breath-hold and free-breathing. For breath-hold imaging, acquiring multiple arterial phase images in a breath-hold is the preferred approach over conventional single-phase imaging. For free-breathing imaging, a combination of three-dimensional (3D) stack-of-stars golden-angle sampling and compressed sensing parallel imaging reconstruction is one of emerging techniques. Self-gating can be used to decrease respiratory motion artifact. This article introduces recent MRI technologies relevant to hepatic arterial phase imaging, including differential subsampling with Cartesian ordering (DISCO), golden-angle radial sparse parallel (GRASP), and X-D GRASP. This article also describes techniques related to dynamic 3D image reconstruction of the liver from golden-angle stack-of-stars data.

Keywords: Dynamic contrast enhanced MRI; Liver; Image reconstruction; Pulse sequence; Compressed sensing; GRASP

INTRODUCTION

Hepatocellular carcinoma (HCC) is the most primary malignant cancer of the liver. It has high incidence rates in Eastern Asia (1, 2). Its incidence is increasing in the United States (2). Dynamic contrast enhanced (DCE) liver magnetic resonance imaging (MRI) with multi-detector computed tomography (CT) plays an important role in detecting and characterizing primary and metastatic lesions (3, 4), including HCC (5). A DCE liver MRI protocol consists of acquisition of a set of volumetric images at pre-contrast, arterial, portal venous, and delayed phases as illustrated in Figure 1. Other non-contrast enhanced images such as diffusion weighted imaging (DWI) and T2-weighted imaging are helpful for the diagnosis. Thus, they are acquired along with DCE imaging in a routine abdominal scan protocol. In portal venous and delayed phases, contrast enhancement becomes relatively stationary over time. A static three-dimensional (3D) imaging is performed within a breath-hold to robustly image the liver without respiratory motion artifact. Fast 3D imaging with sub-Nyquist sampling and parallel

imaging is helpful in reducing scan time while maintaining spatial resolution and anatomic coverage. A combined use of compressed sensing and parallel imaging has potential to further reduce the scan time.

Regardless of the type of contrast agent (either extracellular or hepatobiliary agent), the arterial phase is characterized by rapid enhancement of MR signal in the liver. Due to its transient nature, image acquisition needs to be sufficiently fast as well as well-timed. Thus, arterial phase is more challenging than other phases. High spatio-temporal resolution dynamic imaging is desirable for capturing hemodynamics of lesion enhancement. However, its trade-offs of anatomic coverage, spatial resolution, and temporal resolution need to be compromised given

limitations of MR hardware and subject's breath-hold capability. In this article, recent MR imaging strategies for DCE arterial phase imaging in the liver are discussed. They can be largely divided into two categories: breath-hold imaging and free-breathing imaging. Selected publications and image acquisition techniques for arterial phase imaging are summarized in Table 1. Subsequent sections describe imaging technologies in detail.

BREATH-HOLD IMAGING

Breath-hold imaging is intended to acquire images free from respiratory motion. Scan time is limited by the length

Table 1. Summary of Selected Image Acquisitions for Arterial Phase Imaging

Respiratory control	Publications	Scanner	Field strength	Sequence	No. of phases	ACQ time (sec)	Contrast agent	Advantage	Disadvantage
BH	Michaely et al., 2013 (48)	Siemens Skyra	3T	Cartesian (CDT-VIBE)	14	29	Gd-DOTA (extracellular)	High spatio-temporal resolution (1.2 × 1.2 × 3.0 mm^3, 2.1 sec), robust fat suppression	Long BH time
	Hope et al., 2013 (9)	GE MR750	3T	Cartesian (DISCO)	5	25	Gadoxetic (hepatobiliary)	No need of bolus timing technique, robust fat suppression	Long BH time
	Fujinaga et al., 2014 (13)	Siemens Trio	3T	Radial (r-VIBE-KWIC)	8	20-24	Gadoxetic (hepatobiliary)	Less susceptible to motion than Cartesian	Longer BH time than Cartesian VIBE
	Ichikawa et al., 2018 (10)	GE MR750	3T	Cartesian (DISCO)	6	22-26	Gadoxetic (hepatobiliary)	Ring-like enhancement in HCC visualization better than single phase imaging	Longer BH time than single phase imaging
FB	Chandarana et al., 2013 (14)	Siemens Verio	3T	Radial (GRASP)	N/A	90	Gadopentetate dimeglumine (extracellular)	Flexible retrospective selection of temporal resolution	No respiratory motion correction
	Chandarana et al., 2015 (17)	Siemens Avanto	1.5T	Radial (XD-GRASP)	N/A	318-340	Gadoxetic (hepatobiliary)	Multiphase images with additional respiratory motion states	Potential increase in reconstruction and processing time
	Kaltenbach et al., 2017 (30)	Siemens Prisma	3T	Cartesian (XD-VIBE)	16	188	Gadobutrol (extracellular)	Reconstruction complexity lower than XD-GRASP	Longer reconstruction time than CS-VIBE
	Weiss et al., 2018 (31)	Siemens Aera	1.5T	Cartesian (CS-VIBE)	16	128	Gadobutrol (extracellular)	Reconstruction complexity lower than XD-VIBE	More pronounced artifacts than XD-VIBE
	Yoon et al., 2018 (26)	Siemens Skyra	3T	Radial (GRASP)	N/A	210	Gadoxetic (hepatobiliary)	No TSM artifacts in patients showing TSM in BH imaging	No respiratory motion correction

ACQ = acquisition; BH = breath-hold; CDT-VIBE = CAIPIRINHA-dixon-twist volume-interpolated breath-hold examination; CS = compressed sensing; DISCO = differential subsampling with cartesian ordering; FB = free breathing; GRASP = golden-angle radial sparse parallel imaging; HCC = hepatocellular carcinoma; KWIC = k-space weighted image contrast; N/A = not available; T = tesla; TSM = transient severe motion

of a breath-hold, approximately 12-15 s in clinical exams. Arterial enhancement is rapid. It is desirable to perform imaging within a narrow temporal window. Hence, a proper coordination of imaging and breath-hold timing between MRI operator and patient is critical for the success of breath-hold arterial phase imaging.

Timing of the arterial phase image acquisition can be adjusted based on real-time MR fluoroscopy. In real-time MR fluoroscopy, a 2D slice in the descending aorta or other regions of interest is imaged at every second and the actual 3D arterial phase imaging is initiated when the contrast enhancement from MR fluoroscopy is observed. Meanwhile, a simple approach is to pre-determine a time delay between the start of bolus injection and the time of peak aortic enhancement and take account of the time delay for actual arterial phase imaging. Fixed delay time method may produce sub-optimal lesion enhancement in images of certain patients. Test-injection method is an alternative approach that estimates a delay interval of patient-specific time-to-peak aortic enhancement with a test bolus for an individual patient. It uses the delay interval to acquire k-space center at lesion enhancement in the patient. The test-injection method has been demonstrated to be able to improve lesion conspicuity over the fixed delay time method in breath-hold arterial phase imaging (6), although a drawback of the method is that an additional dosage of contrast agent is needed.

A simple and conventional imaging protocol is to apply the same breath-hold single phase 3D imaging sequence to the pre-contrast, arterial phase, portal venous phase, and delayed phase (Fig. 1a). A T1-weighted 3D radiofrequency (RF) spoiled gradient echo sequence with fat suppression is the most commonly used sequence. It is referred to as eTHRIVE (enhanced T1 high resolution isotropic volume excitation; Philips), VIBE (volumetric interpolated breath-hold examination; Siemens), and LAVA-Flex (liver acquisition with volume acquisition; GE). However, the breath-hold single phase imaging during the arterial phase is known to be problematic in some cases partly because of image quality degradation.

Multiple phase imaging is a viable approach to potentially resolve the image quality issue raised by single-phase imaging. It is designed to reduce temporal window per frame. It possibly allows one to select an image frame free of motion artifact (7). DISCO (differential subsampling with Cartesian ordering) is based on random sub-sampling of the k-space periphery (Fig. 2). It has been demonstrated in hepatic arterial imaging within a breath-hold (8,

9). Six-phase (10) and seven-phase (11) acquisitions using DISCO have also been demonstrated. CAIPIRINHA (controlled aliasing in parallel imaging technique results in higher acceleration; Siemens) has been used in a 3D spoiled gradient echo to achieve higher acceleration than conventional parallel imaging (12). It has been shown that radial imaging with KWIC (k-space weighted image contrast) view-sharing technique can obtain eight phases, with each phase having 2.5-3.0 s temporal resolution (13).

FREE BREATHING

Free-breathing imaging is well-suited to subjects who are unable to tolerate many repetitions of breath-hold, especially to children or elderly patients. However, respiration can cause motion in the diaphragm and abdomen, resulting in data inconsistency in k-space data. Minimal respiratory motion is preferred during imaging and the subject is instructed to perform shallow breathing during the scan. To decrease respiratory motion during free-breathing, navigator signals can be acquired along with imaging data or respiration belts can be used to track respiration dynamics and prospectively acquire data only during a certain respiratory phase. This approach is helpful in reducing respiratory motion artifacts in reconstructed images. However, it also reduces k-space sampling efficiency or image acquisition speed.

In free-breathing liver imaging, an early approach does not consider correcting respiratory motion. It uses continuous golden-angle radial acquisition and compressed sensing parallel imaging reconstruction to improve spatio-temporal resolution (14). This technique is referred to as GRASP (golden-angle radial sparse parallel) (15). Continuous data acquisition with GRASP is an emerging technique as it is flexible in retrospectively selecting temporal resolution and the center of temporal window (Figs. 3, 4).

Respiratory motion can be reduced if one can extract respiratory information from raw data itself (i.e., self-gating), properly bin the raw data into respiratory phases, and finally perform image reconstruction from the data in each respiratory bin. Figure 5 illustrates processes related to binning raw data into respiratory phases using raw data acquired from a GRASP sequence. XD-GRASP adds an additional dimension related to respiratory motion state to an image to be reconstructed and exploits transform sparsity in the respiration dimension (16) to achieve higher acceleration. The framework is helpful in resolving

respiratory phases and recovering images with reduced respiratory motion artifacts. XD-GRASP in hepatic arterial imaging has been demonstrated previously (17).

CONTRAST AGENTS

There are largely two different types of gadolinium-based contrast agents used in DCE liver MRI: extracellular contrast agents and hepatobiliary contrast agents. Extracellular agents allow diagnosis of HCC based on vascularity only
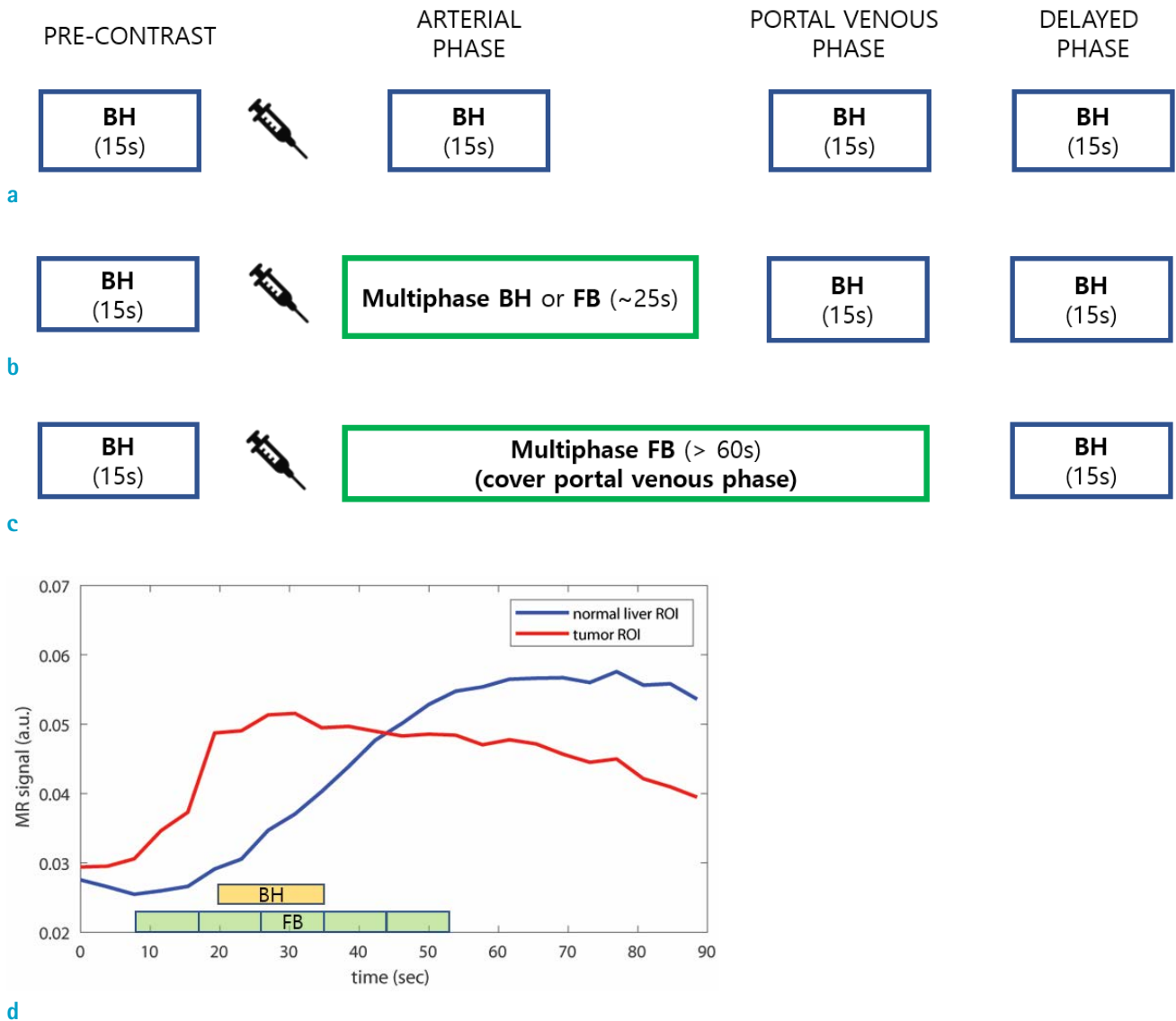

Fig. 1. DCE liver MRI scan protocols. (a) Schematic of a conventional DCE liver imaging protocol. All acquisition sequences have the same single-phase 3D fast gradient echo (GRE), which is referred to as eTHRIVE for Philips, VIBE for Siemens, and LAVA for GE, acquired within a breath-hold (BH), typically lasting for 15 seconds. (b) Schematic of a modified protocol where a multi-phase imaging method (green box) is substituted for the conventional single-phase acquisition of arterial phase. BH: breath-hold; FB: free-breathing. (c) Schematic of a modified protocol where a multi-phase FB imaging (green box) is used and the duration of FB imaging is extended to cover the portal venous phase. (d) Time versus MR signal curves from normal liver region of interest (ROI) and tumor ROI. The orange box indicates the acquisition time interval of single-phase BH imaging and the green box shows that of multi-phase FB imaging. In single-phase BH imaging, start time of the acquisition is critical for differentiation of tumor enhancement from normal tissue.

iMRI

while hepatobiliary contrast agents allow diagnosis of HCC based on both vascularity and hepatocellular functions. The important advantage of hepatobiliary agents over extracellular agents is that hepatobiliary agents are capable of assessing hepatocellular function to help detect hypovascular and small HCCs (i.e., early stage HCCs) in delayed hepatobiliary phase (18-20).

Gadoxetate disodium (gadoxetic acid; Gd-EOB-DTPA; Primovist, Bayer Schering Pharma; Eovist, Bayer HealthCare) and gadobenate dimeglumine (MultiHance, Bracco) are two different types of hepatobiliary agents. Gadoxetate disodium is more frequently used than gadobenate dimeglumine in clinical liver imaging as it affects higher hepatocellular uptake and results in shorter time needed to reach hepatobiliary parenchymal enhancement (i.e., 20 minutes delay vs. 1-3 hours delay) (18). Hence, delayed hepatobiliary imaging with gadoxetate disodium occurs earlier than that with gadobenate dimeglumine. For comparison, delayed phase imaging with extracellular agents typically occurs 3-5 minutes after the injection of contrast agents.

Although gadoxetate disodium is beneficial due to potentially high sensitivity of tumor detection in delayed hepatobiliary phase, arterial phase imaging with gadoxetate disodium is known to be more challenging than arterial phase imaging with extracellular agents (21). Recommended dose of gadoxetate disodium is 0.025 mmol/kg, four times lower than the recommended dose (0.1 mmol/kg) of extracellular agents. Although gadoxetate disodium

has a higher relaxivity, the overall signal enhancement of gadoxetate disodium is lower due to its low dose than extracellular agents. Because of its low dose usage, time window of arterial phase contrast enhancement is relatively narrow in gadoxetate disodium. Hence, it is likely to miss the image acquisition time for conventional single-phase breath-hold imaging. Although higher dose of gadoxetate disodium may improve contrast to noise ratio, it is likely to increase the risk of transient severe motion (TSM) in arterial phase imaging (22). TSM in gadoxetic acid agents is observed more frequently than that in other extracellular agents when a standard breath-hold imaging is used (23-25). It has been reported that free-breathing imaging with GRASP can provide acceptable image quality of arterial phases in patients with TSM (26).

IMAGE ACQUISITION

Cartesian Sampling

Cartesian imaging acquires k-space data on a uniformly spaced Cartesian grid. It is the most commonly used sampling scheme in clinical MR exams. Since arterial phase imaging requires time-efficient imaging strategies, pulse sequence has been developed to highly undersample on the Cartesian grid while maintaining diagnostic image quality.

TRAK (time-resolved angiography with keyhole; Philips), TWIST (time-resolved angiography with stochastic
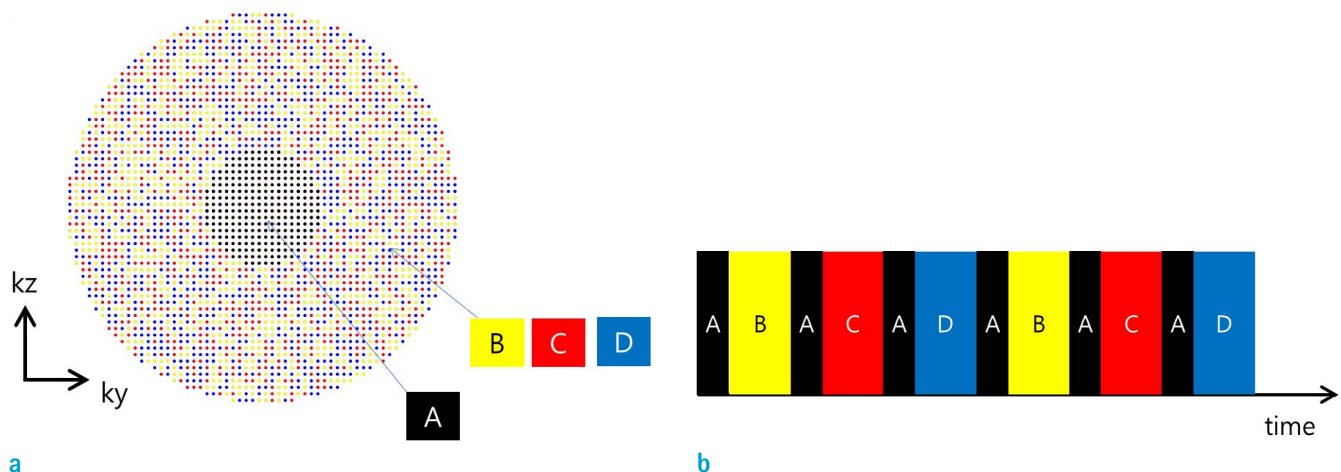

Fig. 2. Schematic illustration of DISCO. (a) Sampling distribution. Section A is fully sampled in (ky, kz) while sections B, C, and D are under-sampled in a pseudo-random manner. The union of samples from sections B, C, and D is fully sampled. (b) Temporal acquisition order of the k-space sections. Note that section A is acquired more frequently in time than sections B, C, and D.

trajectories; Siemens), and TRICKS (time-resolved imaging of contrast kinetics; GE) are frequently used to sample the central sector in (ky, kz) (i.e., phase-encode and slice-encode) and sub-sample peripheral sectors. They use view sharing for image reconstruction where frame rate is determined by the frequency of acquisition of the central
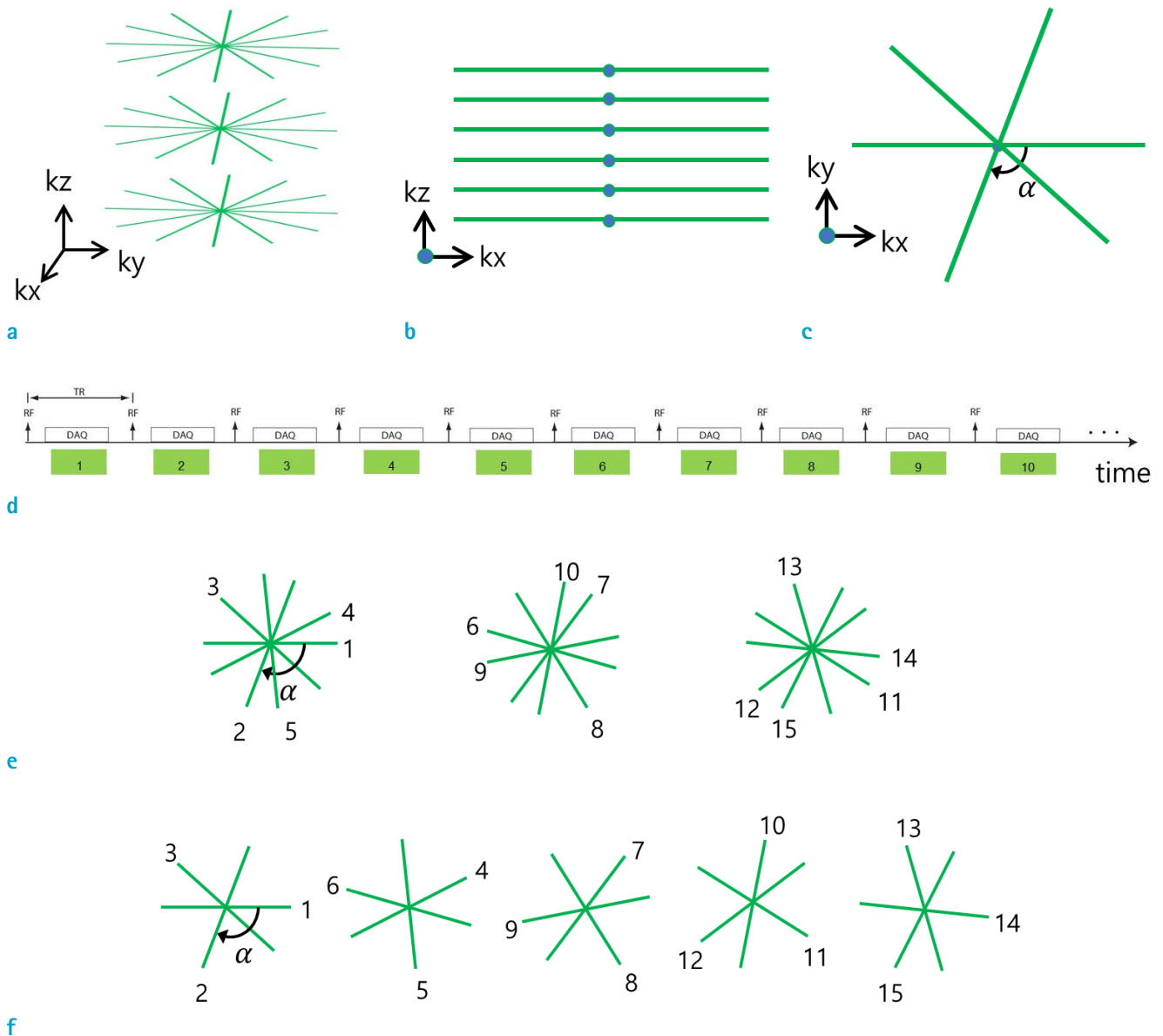

Fig. 3. Schematic illustration of 3D GRASP. (a) 3D view of k-space sampling pattern. (b) 2D view in (kx, kz). (c) 2D view in (kx, ky). For a given angle spoke, it samples uniformly in kz axis until it fills out the kz space. The spoke angle is then incremented by golden angle α ≈ 180°/1.618 ≈ 111°, followed by filling out the kz space. This process is repeated until it reaches the prescribed number of radial spokes. (d) Continuous imaging sequence in 2D golden-angle radial sequence. The same principle can also be applied to 3D GRASP without loss of generality. The number in the green box indicates spoke order. (e, f) Sampling patterns after retrospective selections of temporal window by grouping (e) five consecutive spokes per frame and (f) three consecutive spokes per frame. For both cases (one with grouping of 5 spokes and the other with grouping of 3 spokes), patterns of angle spacing in radial spokes are similar in all frames. This is relevant to the fact that golden angle radial sampling guarantees temporal stability. Per frame basis, (e) is more densely sampled (less spatial aliasing) than (f). (e) has a lower frame rate than (f).

sector. TRAK, TWIST, and TRICKS differ in how sub-sampling in the k-space periphery is distributed temporally (8, 27).

DISCO (8, 9, 28) is based on a variable density undersampling scheme in (ky, kz), in which a pseudo-random distribution is generated in the periphery of (ky, kz) space and the central region is fully sampled (Fig. 2). Since pseudo-random undersampling promotes incoherency in aliasing, it is well suited to compressed sensing reconstruction (29). Notably, incoherent variable density Cartesian sampling (referred to as CS VIBE or VIBECS) has been recently demonstrated to have compressed sensing in free-breathing DCE liver imaging (30, 31)

Radial Sampling

Radial sampling covers the k-space by acquiring k-pace lines, each of which passes through the k-space origin. It is less sensitive to motion than Cartesian sampling since it samples the k-space origin, in which signal intensity is concentrated, more frequently than Cartesian sampling. However, it is sensitive to hardware imperfections such as gradient timing delays (32) and eddy currents. In the presence of off-resonance, image quality can be degraded and manifested as spatial blurring (33). Inherently, in radial sampling, low spatial frequency in k-space is more densely sampled than high spatial frequency portion. When it is
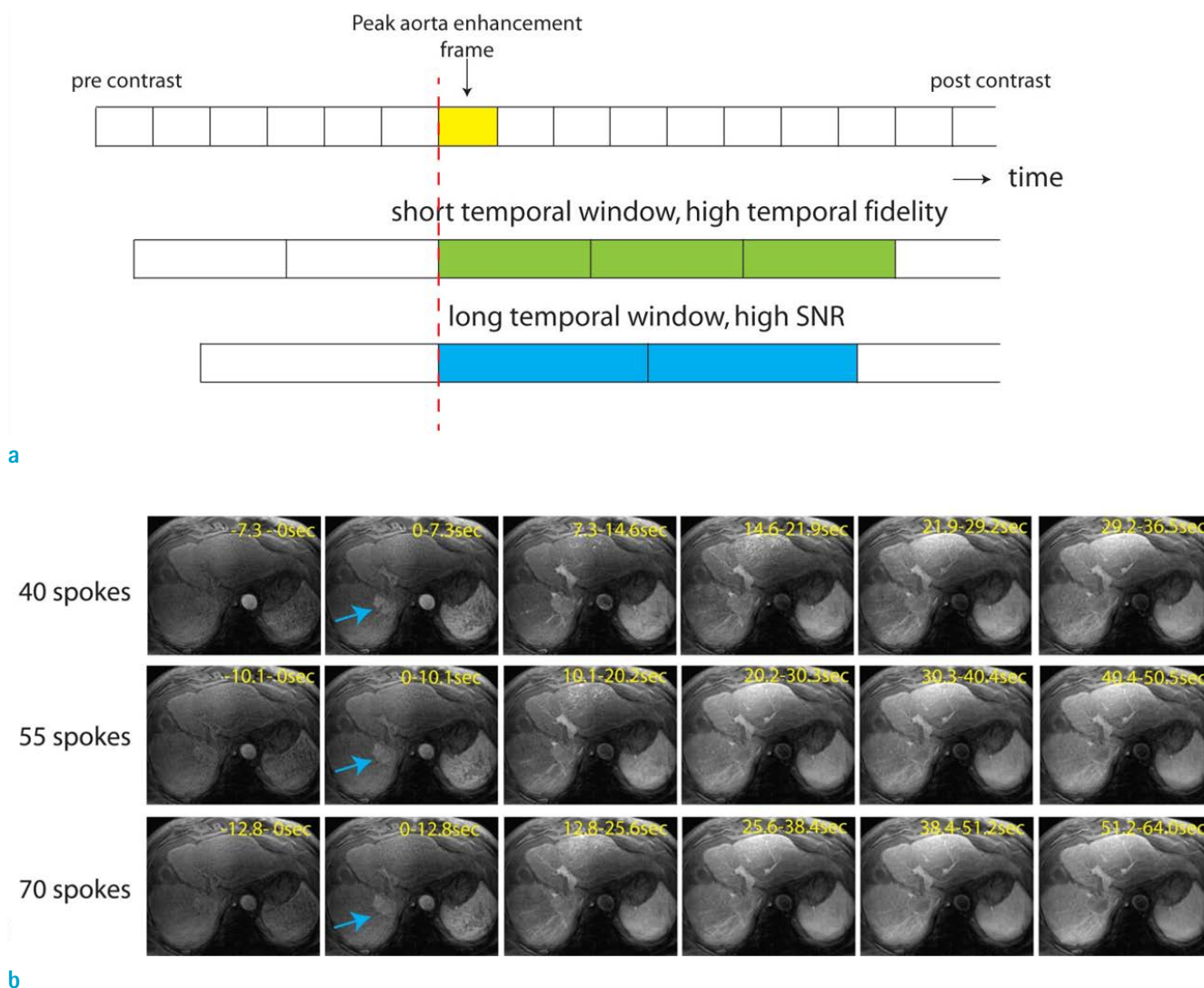
a

b

Fig. 4. Retrospective reconstructions from GRASP data. (a) Schematic of retrospective adjustment of a starting point (red dashed line) and temporal window (green and blue) from continuously acquired raw data in GRASP. (b) Retrospective reconstructions with choices of 40, 55, and 70 spokes. Results exhibit stable image reconstruction quality in all frames for the three cases.

under-sampled, the aliasing appears like streak artifact rather than fold-over artifact manifested by Cartesian undersampling. However, the structure of an object is often noticeable to human eyes. Undersampled streak artifact
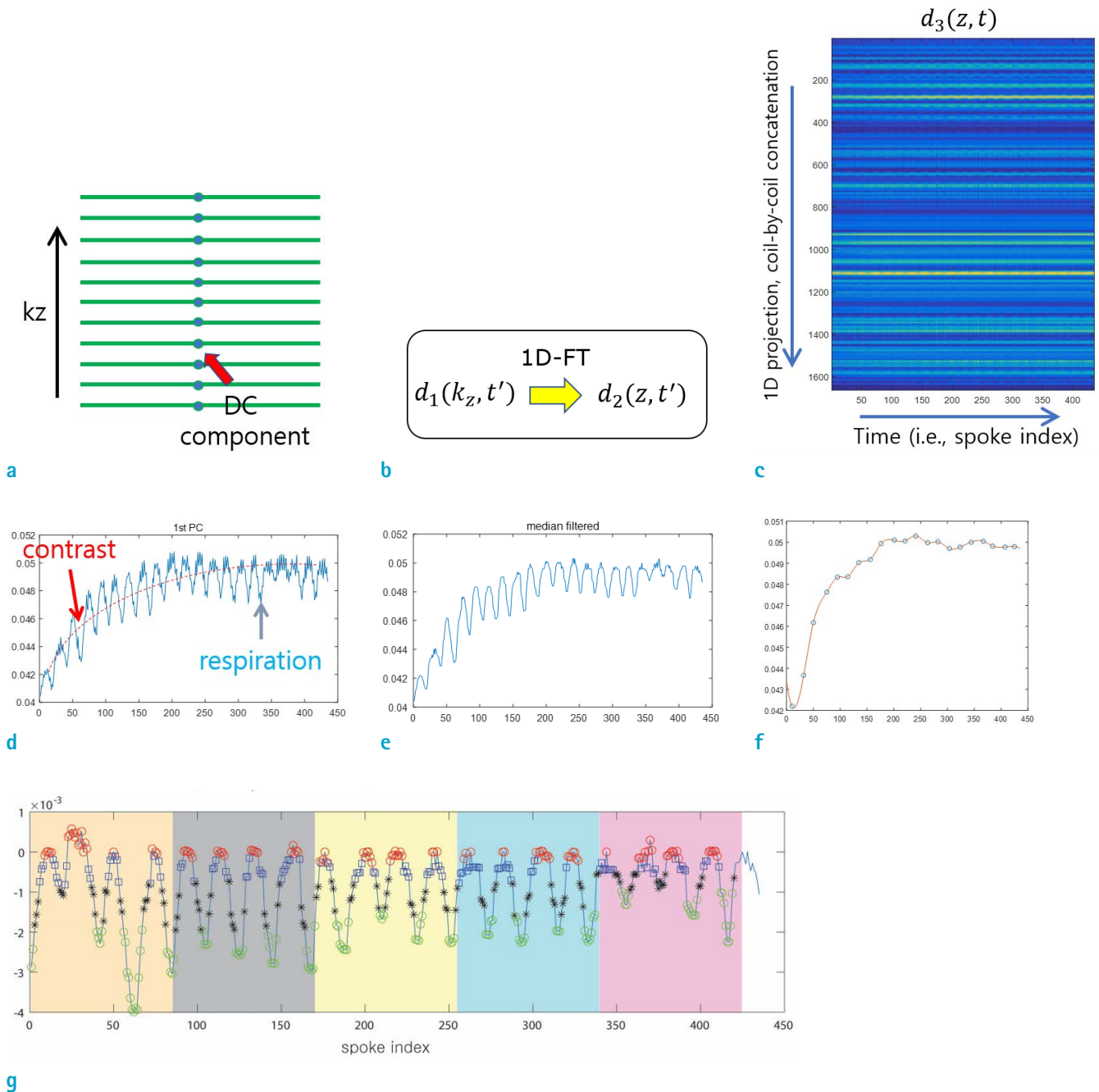

g

Fig. 5. Illustration of data binning procedures in XD-GRASP. (a) Raw data samples at the center in (kx, ky) are extracted for each spoke t' and are denoted by $d_1(kz, t')$. (b) One-dimensional Fourier transform is performed along kz to transform data $d_1(kz, t')$ to $d_2(z, t')$ for each spoke t'. $d_2(z, t')$ represents 1D projection signal projected to superior-inferior (S-I) direction. (c) Construction of a 2D image $d_3(z, t)$ by concatenating 1D projection data for all coils and all radial spokes. (d) A result of the first principal component after performing principal component analysis (PCA) of the 2D image $d_3(z, t)$. (e) A result of smooth version of (d) after taking a median filter in time. (f) Estimation of the envelope (red line) after a spline fitting to peak points in (e). (g) Flattened curve after division of (e) by (f). Final motion state assignment is indicated by different colors (state 1: red, state 2: blue, state 3: black, state 4: green). Contrast phases are differentiated by background colors in the plot.

appears overlaid to the structure of an object. Compressed sensing parallel imaging reconstruction is highly effective in removing the streak artifact and recovering alias free images (34).

In dynamic radial imaging, high spatial frequency data from adjacent temporal frames can be exploited to fill out unacquired k-space locations in a current temporal frame. KWIC (35) is a reconstruction technique that can achieve high frame rate imaging with substantially reduced aliasing by taking advantage of the fact that unacquired

high spatial frequency data can be filled in by those of adjacent temporal frames without causing significant loss of temporal fidelity.

Radial sampling has gained more popularity in research and clinical domains thanks to the introduction of golden-angle radial sampling framework (36). Golden angle sampling simply increments the angle of radial spoke by the golden angle at every repetition time (TR) (36). GRASP adopts golden-angle radial sampling for volumetric imaging (Fig. 3) and accelerates imaging speed by using
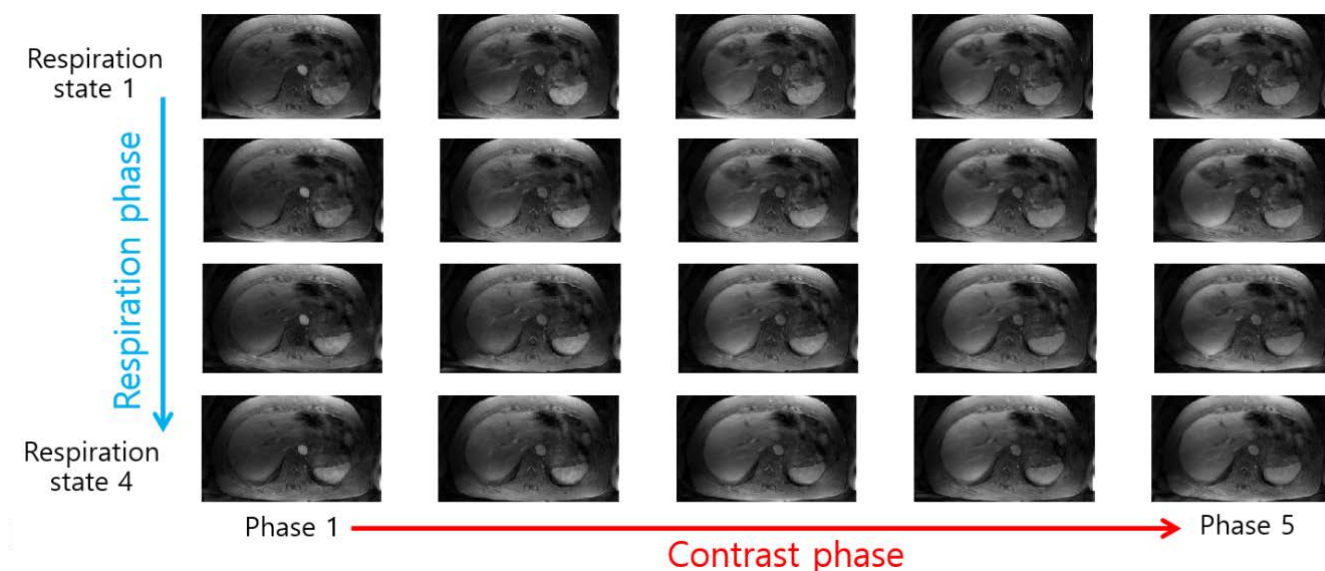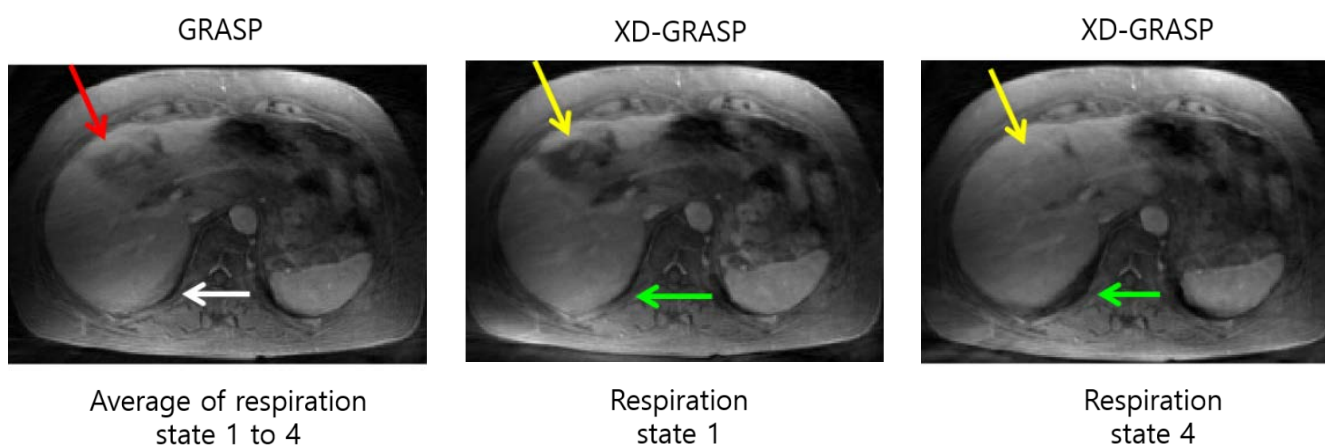
Fig. 6. An example of reconstructed images using XD-GRASP. (a) Final reconstructed images of XD-GRASP. These images contain an additional respiratory motion-resolved dimension. (b) Comparison of GRASP and XD-GRASP for contrast phase 5. GRASP exhibits an image of averaged motion from all respiration states. XD-GRASP contains images, each of which is from a respiration state. Note that there are differences in image appearance between respiration states 1 and 4 (yellow and green arrows). Also note motion-averaged image appearance in the GRASP image (red and white arrows).

compressed sensing parallel imaging reconstruction from highly undersampled data (15). An advantage of continuous golden angle radial imaging is that reconstructed images exhibit temporal stability for all frames given any arbitrary choice of temporal offset and temporal window (37) (Fig. 4).

Alternatively, pseudo-golden angle radial sampling that is also referred to as radial-eTHRIVE (Philips) can be designed to acquire k-space lines by angle increments close to the golden angle, although sample may have azimuthally and uniformly distributed spokes in k-space. Hence, in case of static single-phase imaging, pseudo-golden angle sampling can theoretically produce less streak artifact than conventional golden angle sampling. It has potential to produce less motion artifact than conventional Cartesian imaging (38, 39).

In 3D imaging using radial sampling, there are largely two approaches: 1) 3D stack-of-stars (e.g., GRASP), and 2) pure 3D radials (a.k.a., Kush-ball). In 3D stack-of-stars, the principle of 2D radial sampling is applied to (kx, ky) space while Cartesian sampling is applied in kz space. Straightforwardly, 3D golden-angle stack-of-stars acquisition samples the (kx, ky) space following golden angle radial trajectories and the kz space uniformly (Fig. 3). Partial Fourier sampling is often applied to kz encode to increase acquisition speed. The 3D radial projection sampling (i.e., Kush-ball) is used less often than 3D stack-of-stars sampling due to the need for a compact field-of-view setting the slice encode and sampling inefficiency of pure 3D radials. Imaging based on 3D radial projection sampling in time-resolved imaging of the liver in DCE MRI
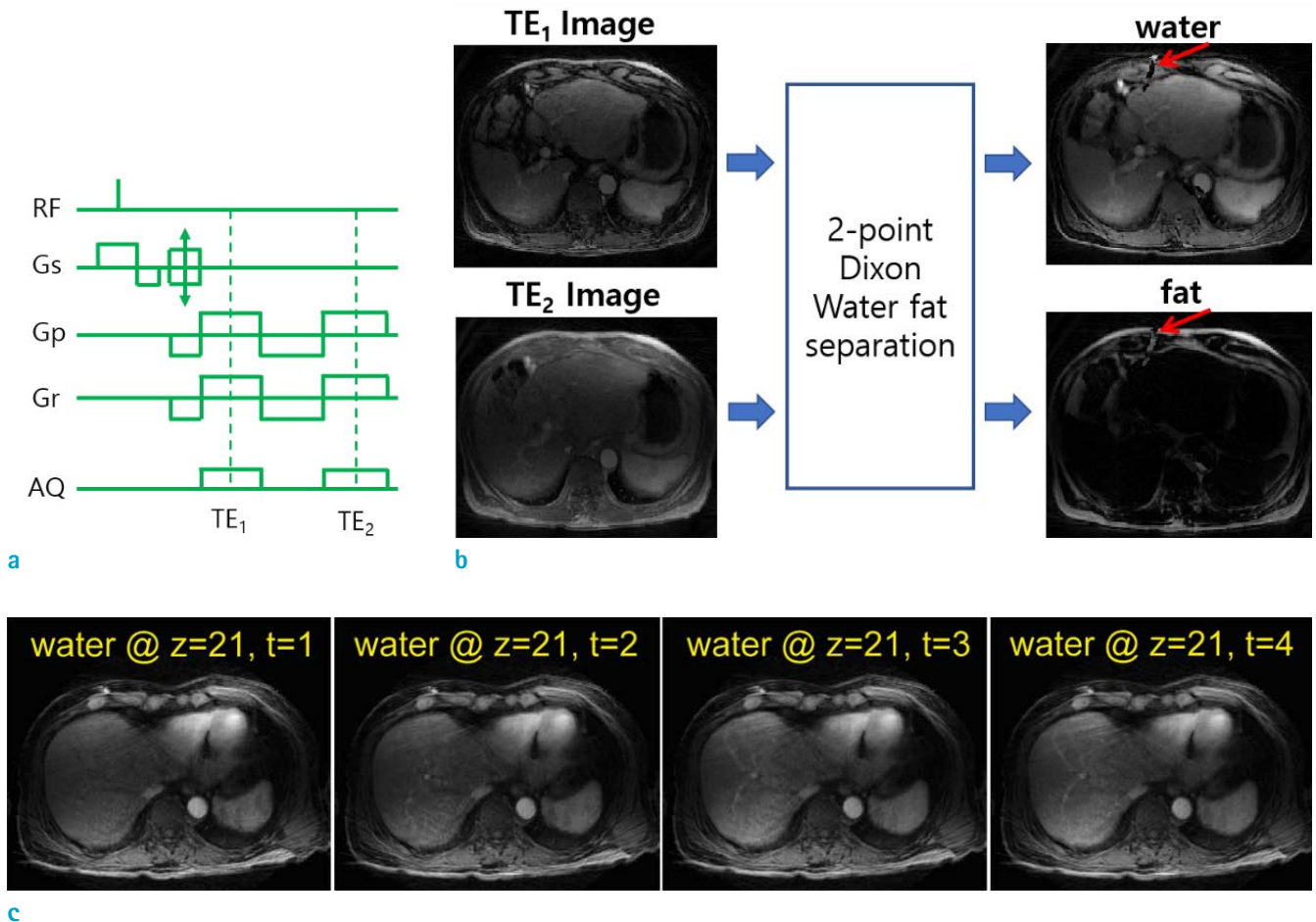

Fig. 7. Illustration of water fat separation from continuously acquired dual-echo 3D stack-of-stars golden-angle radial raw data. (a) Schematic of a radial dual-echo pulse sequence. (b) TE$_1$ and TE$_2$ images can be separately reconstructed using compressed sensing and parallel imaging. These complex-valued images are input to a 2-point Dixon water fat separation algorithm. The output is a set of water and fat images. Water-fat swap artifact is indicated by red arrows. (c) Final fat suppressed dynamic image frames are shown.

has been demonstrated (40).

Spiral Sampling

Spiral sampling is less sensitive to motion than Cartesian sampling since the spiral trajectory traverses the k-space center at every TR. A major drawback of spiral imaging is that it suffers from image blurring and distortion due to off-resonance and hardware imperfections (41). Correction of these artifacts may be subject to MR operator's trial and error of parameter tuning, thus potentially lacking reproducibility of the same image quality or lengthening the exam time. This is regarded as a main obstacle to adoption of spiral imaging for clinical exams, especially in high-field MRI. A 3D golden-angle stack-of-spirals imaging technique (i.e., spiral encoding in [kx, ky] and Cartesian encoding in [kz]) with 3-second temporal resolution in hepatic arterial phase imaging at 1.5 Tesla (T) has been demonstrated (42, 43).

Controlled Aliasing in Parallel Imaging

CAIPIRINHA (44, 45) is a modification of conventional parallel imaging by changing image acquisition and reconstruction scheme. In 2D parallel accelerations in 3D imaging, CAIPIRINHA is advantageous over conventional parallel imaging with regard to signal-to-noise ratio (SNR) for high acceleration factors (46, 47). CAIPIRINHA has been used by numerous groups for clinical 3D DCE liver imaging (12, 48-50). A sequence referred to as CAIPIRINHA-Dixon-TWIST (CDT) VIBE, as the name implies, adopts CAIPIRINHA in DCE arterial phase imaging in the liver (48). Acquisition of dynamic 3D images with 2.6 sec temporal resolution within a single breath-hold has been demonstrated (48).

IMAGE RECONSTRUCTION

Compressed Sensing Parallel Imaging

Image reconstruction in compressed sensing parallel imaging can be posed as an optimization problem where a data consistency term is related to fitting of measured data to an MR signal model and a regularization term promotes sparsity in transform domain. Eq. [1] describes an example of optimization formulation for estimating an image $\widehat{m}$.

$$\widehat{m} = \underset{m}{\mathrm{argmin}} \, ||F{\cdot}C{\cdot}m{-}d||_2^2 + \lambda_1||S_1{\cdot}m||_1, \qquad \text{Eq. [1]}$$

where m is 3D dynamic image in x-y-z-t, C is coil sensitivity, F is undersampled Fourier encoding, d is undersampled

k-space data in kx-ky-kz-t-coil, S_1 is temporal sparsifying transform operator, and λ_1 is a regularization parameter. Temporal L1-norm regularization is highly effective in reducing incoherent aliasing artifact from pseudo-randomly undersampled data in Cartesian sampling such as DISCO or in reducing streak artifact reconstructed from highly undersampled radial data such as GRASP.

In Cartesian acquisition such as DISCO, frequency encode (i.e., kx) is fully sampled. In practice, to save memory space, k-space data can be Fourier-transformed along kx to obtain k-space data in x-ky-kz-t-coil. For a given x, an image series in y-z-t can be reconstructed. Coil sensitivity maps can be derived from fully sampled central portion in (ky, kz).

In 3D stack-of-stars acquisition such as GRASP, slice encode (i.e., kz) is fully sampled (or often performed in partial k-space where the acquired sample spacing meets the Nyquist sampling criterion). In practice, to save memory space, k-space data can be Fourier- transformed along kz to obtain k-space data in kx-ky-z-t-coil. For a given z, an image series in x-y-t can be reconstructed. Coil sensitivity maps can be derived from densely sampled central portion in (kx, ky).

Respiration as an Additional Dimension

In free-breathing continuous acquisition, images can be reconstructed with respiratory motion as an additional dimension. Eq. [2] describes an example of optimization formulation for estimating an image $\widehat{m}$.

$$\widehat{m} = \underset{m}{\mathrm{argmin}} \, ||F{\cdot}C{\cdot}m{-}d||_2^2 + \lambda_1||S_1{\cdot}m||_1 + \lambda_2||S_2{\cdot}m||_1, \quad \text{Eq. [2]}$$

where m is the respiratory motion resolved 3D dynamic images in x-y-z-t-r, C is coil sensitivity, F is undersampled Fourier encoding, d is undersampled k-space data sorted based on respiratory motion in kx-ky-kz-t-coil-r, S_2 is sparsifying transform operator along respiratory motion state, and λ_1 and λ_2 are regularization parameters. Figure 6 demonstrates X-D GRASP reconstructed images that contain respiration states for all contrast phases. X-D reconstruction framework in a variable density Cartesian sampling scheme with 1-D navigation sequence has also been demonstrated (30).

FAT SUPPRESSION

Adipose tissue, or fat, has unique characteristics in MR imaging. First, fat has short T1 recovery time. Second,

fat has a distinct resonance frequency offset known as chemical shift. Because T1 of fat is short, fat signals appear bright in images acquired with a T1-weighted gradient echo sequence. The brightness of fat may not be well-differentiated from the brightness of lesions in arterial phase imaging. Hence, fat suppression is important to improve lesion conspicuity. There are two methods that can suppress fat: fat saturation and water-fat separation.

Fat Saturation

Fat saturation pulses can be applied before imaging pulses to suppress fat. As 3T MRI is increasingly used over 1.5T for liver imaging, fat suppression pulses that are robust to B_0 and B_1 field inhomogeneity are advantageous. SPAIR (spectrally adiabatic inversion recovery; Siemens) uses a 180° fat-selective adiabatic inversion pulse for the robustness to B_1 field inhomogeneity and nulls fat signal at imaging. SPIR (spectral pre-saturation with inversion recovery; Philips) is based on a 110-180° fat-selective inversion recovery and nulling of fat signal at imaging. SPAIR or SPIR is typically used in conventional single breath-hold 3D DCE liver imaging. For a longer acquisition lasting beyond a single breath-hold which is attempted in arterial phase imaging, fat saturation pulses need to be periodically applied to maintain adequate fat suppression (51). A drawback of this approach is that images are not acquired during fat saturation preparation pulses.

Water-Fat Separation

Water-fat separation (a.k.a., Dixon technique) is an alternative approach for fat suppression. It takes advantage of chemical shift property of fat. A thorough review of water-fat separation has been provided by Eggers and Bornert (52). Typically, in-phase, oppose-phase, water and fat images are obtained after processing. Since data are acquired with more than one echo, TR is longer than the single echo sequence. Dual echo imaging is advantageous over triple echo imaging in DCE liver MRI because it is faster due to the use of shorter TR. Echo time can be flexibly adjusted and shortened to reduce TR (53, 54). For arterial phase imaging of long acquisition time, dual echo Dixon imaging may be more suitable than imaging with fat saturation preparation pulses since imaging can be continuous without needing preparation pulses. Figure 7 illustrates water-fat separation from dual-echo GRASP data. Although not shown in the Figure, with the same dual-echo GRASP data, water-fat separation can be obtained along with respiratory motion resolved when X-D GRASP

reconstruction is performed. In addition, a feasibility of image reconstruction concurrent with water-fat separation has been demonstrated in a recent study by Benkert et al. (55). The method was based on an MR signal model, incorporating chemical shift encoding. It demonstrated that fat suppressed liver images were reconstructed with reduced imaging blurring.

QUANTITATIVE LIVER PERFUSION

Workflow for Quantification

The main goal of quantitative liver perfusion imaging is to separately obtain arterial and portal venous blood flow in the liver (56). Free-breathing T1-weighted dynamic 3D acquisition sequences are typically used with sufficiently long acquisition time encompassing arterial and portal venous phases. Parallel imaging with view sharing is used to increase spatial-temporal resolution. Image registration of dynamic image frames is often necessary to correct for respiratory motion and improve accuracy of liver perfusion quantification (57). MR signal intensity is converted to contrast agent concentration for absolute quantification. Quantification of blood flow can be typically performed based on dual-input single-compartment model and numerical optimization involving deconvolution. Here, "dual-input" implies blood supplies from 1) the hepatic artery and 2) the portal vein. Notably, dual-input two-compartment model, unlike dual-input single-compartment model, assumes extracellular and intracellular compartments in the pharmaco-kinetic modeling. Sourbron et al. (58) have demonstrated the benefit of dual-input two-compartment model in improved data fitting of concentration-time curves. Estimated quantities include arterial flow, venous flow, arterial fraction, extracellular volume, and hepatocellular (intracellular) uptake rate.

Accelerated Imaging

Fast 3D imaging with high spatial-temporal resolution is important for accurate estimation of arterial input function, leading to accurate perfusion quantification. Although conventional view-sharing reconstruction schemes can help increase frame update rate, it has limitation of wide temporal footprints due to the use of adjacent temporal frames for k-space filling. A variety of advanced imaging techniques without view sharing can be employed to increase spatial-temporal resolution in perfusion MRI of the liver. For example, through-time spiral GRAPPA with

temporal resolution of 1.6-1.9 sec/volume and scan time of 3.5 min has been used to obtain liver 3D perfusion maps using a dual-input single-compartment model (59). It has been demonstrated that GRASP with temporal resolution of 2.2-2.4 sec/volume and scan time of 5-6 min can quantify liver function such as total plasma flow, portal venous flow, arterial perfusion fraction, and mean transit time using a dual-input two-compartment model (60). The same continuously acquired data with GRASP have been used to obtain images for morphologic assessment with larger temporal window reconstruction (i.e., approximately 10 seconds of temporal resolution). The flexible temporal resolution selections doable in the golden-angle sampling scheme are intriguing because both morphological and functional assessments are feasible without needing additional scan time or additional contrast agent injection.

In conclusion, conventional breath-hold single-phase liver imaging during arterial phase may suffer from low sensitivity of lesion detection related to improper image acquisition timing or artifacts related to transient severe motion mainly caused by hepatobiliary contrast agents. To overcome these aforementioned limitations, researchers have developed multi-phase acquisitions for breath-hold imaging and dynamic continuous acquisitions for free-breathing imaging. Compressed sensing parallel imaging is a key element for improving spatial and temporal resolution. Recent radial imaging techniques such as GRASP and X-D GRASP have enabled free-breathing arterial phase imaging with multiple phases and demonstrated higher frame-rate images and more reliability in capturing arterial enhancement than conventional breath-hold arterial phase imaging. However, due to their flexibility in the selection of temporal resolution and reconstruction parameters, how one can systematically standardize parameter selection remains unclear. A drawback of dynamic compressed sensing parallel imaging reconstruction schemes is its long image reconstruction time which can be a limiting factor in routine clinical exams. Recently, machine learning-based image reconstruction framework has demonstrated its potential to generate image quality similar to compressed sensing parallel imaging and significantly reduce reconstruction time (61). This topic may be relevant to multi-phase DCE liver image reconstruction in the future.

Acknowledgments

REFERENCES

1. Gomaa AI, Khan SA, Toledano MB, Waked I, Taylor-Robinson SD. Hepatocellular carcinoma: epidemiology, risk factors and pathogenesis. World J Gastroenterol 2008;14:4300-4308
2. Mittal S, El-Serag HB. Epidemiology of hepatocellular carcinoma: consider the population. J Clin Gastroenterol 2013;47 Suppl:S2-6
3. Ringe KI, Husarik DB, Sirlin CB, Merkle EM. Gadoxetate disodium-enhanced MRI of the liver: part 1, protocol optimization and lesion appearance in the noncirrhotic liver. AJR Am J Roentgenol 2010;195:13-28
4. Cruite I, Schroeder M, Merkle EM, Sirlin CB. Gadoxetate disodium-enhanced MRI of the liver: part 2, protocol optimization and lesion appearance in the cirrhotic liver. AJR Am J Roentgenol 2010;195:29-41
5. Bruix J, Sherman M; American Association for the Study of Liver Diseases. Management of hepatocellular carcinoma: an update. Hepatology 2011;53:1020-1022
6. Nakamura S, Nakaura T, Kidoh M, et al. Timing of the hepatic arterial phase at Gd-EOB-DTPA-enhanced hepatic dynamic MRI: comparison of the test-injection and the fixed-time delay method. J Magn Reson Imaging 2013;38:548-554
7. Pietryga JA, Burke LM, Marin D, Jaffe TA, Bashir MR. Respiratory motion artifact affecting hepatic arterial phase imaging with gadoxetate disodium: examination recovery with a multiple arterial phase acquisition. Radiology 2014;271:426-434
8. Saranathan M, Rettmann DW, Hargreaves BA, Clarke SE, Vasanawala SS. DIfferential Subsampling with Cartesian Ordering (DISCO): a high spatio-temporal resolution Dixon imaging sequence for multiphasic contrast enhanced abdominal imaging. J Magn Reson Imaging 2012;35:1484-1492
9. Hope TA, Saranathan M, Petkovska I, Hargreaves BA, Herfkens RJ, Vasanawala SS. Improvement of gadoxetate arterial phase capture with a high spatio-temporal resolution multiphase three-dimensional SPGR-Dixon sequence. J Magn Reson Imaging 2013;38:938-945
10. Ichikawa S, Motosugi U, Oishi N, et al. Ring-like enhancement of hepatocellular carcinoma in gadoxetic acid-enhanced multiphasic hepatic arterial phase imaging with differential subsampling with cartesian ordering.

Invest Radiol 2018;53:191-199

11. Clarke SE, Saranathan M, Rettmann DW, Hargreaves BA, Vasanawala SS. High resolution multi-arterial phase MRI improves lesion contrast in chronic liver disease. Clin Invest Med 2015;38:E90-99

12. Ikram NS, Yee J, Weinstein S, et al. Multiple arterial phase MRI of arterial hypervascular hepatic lesions: improved arterial phase capture and lesion enhancement. Abdom Radiol (NY) 2017;42:870-876

13. Fujinaga Y, Ohya A, Tokoro H, et al. Radial volumetric imaging breath-hold examination (VIBE) with k-space weighted image contrast (KWIC) for dynamic gadoxetic acid (Gd-EOB-DTPA)-enhanced MRI of the liver: advantages over Cartesian VIBE in the arterial phase. Eur Radiol 2014;24:1290-1299

14. Chandarana H, Feng L, Block TK, et al. Free-breathing contrast-enhanced multiphase MRI of the liver using a combination of compressed sensing, parallel imaging, and golden-angle radial sampling. Invest Radiol 2013;48:10-16

15. Feng L, Grimm R, Block KT, et al. Golden-angle radial sparse parallel MRI: combination of compressed sensing, parallel imaging, and golden-angle radial sampling for fast and flexible dynamic volumetric MRI. Magn Reson Med 2014;72:707-717

16. Feng L, Axel L, Chandarana H, Block KT, Sodickson DK, Otazo R. XD-GRASP: Golden-angle radial MRI with reconstruction of extra motion-state dimensions using compressed sensing. Magn Reson Med 2016;75:775-788

17. Chandarana H, Feng L, Ream J, et al. Respiratory motion-resolved compressed sensing reconstruction of free-breathing radial acquisition for dynamic liver magnetic resonance imaging. Invest Radiol 2015;50:749-756

18. Choi JY, Lee JM, Sirlin CB. CT and MR imaging diagnosis and staging of hepatocellular carcinoma: part I. Development, growth, and spread: key pathologic and imaging aspects. Radiology 2014;272:635-654

19. Choi JY, Lee JM, Sirlin CB. CT and MR imaging diagnosis and staging of hepatocellular carcinoma: part II. Extracellular agents, hepatobiliary agents, and ancillary imaging features. Radiology 2014;273:30-50

20. Motosugi U, Bannas P, Sano K, Reeder SB. Hepatobiliary MR contrast agents in hypovascular hepatocellular carcinoma. J Magn Reson Imaging 2015;41:251-265

21. Yoon JH, Lee JM, Yu MH, Kim EJ, Han JK. Triple arterial phase MR imaging with gadoxetic acid using a combination of contrast enhanced time robust angiography, keyhole, and viewsharing techniques and two-dimensional parallel imaging in comparison with conventional single arterial phase. Korean J Radiol 2016;17:522-532

22. Davenport MS, Bashir MR, Pietryga JA, Weber JT, Khalatbari S, Hussain HK. Dose-toxicity relationship of gadoxetate disodium and transient severe respiratory motion artifact. AJR Am J Roentgenol 2014;203:796-802

23. Huh J, Kim SY, Yeh BM, et al. Troubleshooting arterial-phase MR images of gadoxetate disodium-enhanced liver. Korean J Radiol 2015;16:1207-1215

24. Davenport MS, Viglianti BL, Al-Hawary MM, et al. Comparison of acute transient dyspnea after intravenous administration of gadoxetate disodium and gadobenate dimeglumine: effect on arterial phase image quality. Radiology 2013;266:452-461

25. Davenport MS, Caoili EM, Kaza RK, Hussain HK. Matched within-patient cohort study of transient arterial phase respiratory motion-related artifact in MR imaging of the liver: gadoxetate disodium versus gadobenate dimeglumine. Radiology 2014;272:123-131

26. Yoon JH, Lee JM, Yu MH, et al. Evaluation of transient motion during gadoxetic acid-enhanced multiphasic liver magnetic resonance imaging using free-breathing golden-angle radial sparse parallel magnetic resonance imaging. Invest Radiol 2018;53:52-61

27. Min JH, Kim YK, Kang TW, et al. Artifacts during the arterial phase of gadoxetate disodium-enhanced MRI: multiple arterial phases using view-sharing from two different vendors versus single arterial phase imaging. Eur Radiol 2018;28:3335-3346

28. Hope TA, Petkovska I, Saranathan M, Hargreaves BA, Vasanawala SS. Combined parenchymal and vascular imaging: high spatiotemporal resolution arterial evaluation of hepatocellular carcinoma. J Magn Reson Imaging 2016;43:859-865

29. Lustig M, Donoho D, Pauly JM. Sparse MRI: the application of compressed sensing for rapid MR imaging. Magn Reson Med 2007;58:1182-1195

30. Kaltenbach B, Bucher AM, Wichmann JL, et al. Dynamic liver magnetic resonance imaging in free-breathing: feasibility of a cartesian T1-weighted acquisition technique with compressed sensing and additional self-navigation signal for hard-gated and motion-resolved reconstruction. Invest Radiol 2017;52:708-714

31. Weiss J, Notohamiprodjo M, Martirosian P, et al. Self-gated 4D-MRI of the liver: initial clinical results of continuous multiphase imaging of hepatic enhancement. J Magn Reson Imaging 2018;47:459-467

32. Peters DC, Derbyshire JA, McVeigh ER. Centering the projection reconstruction trajectory: reducing gradient delay errors. Magn Reson Med 2003;50:1-6

33. Block KT. Advanced methods for radial data sampling in MRI. Ph.D. thesis, Georg-August-Universitaet Goettingen, 2008

34. Block KT, Uecker M, Frahm J. Undersampled radial MRI with multiple coils. Iterative image reconstruction using a total variation constraint. Magn Reson Med 2007;57:1086-1098

35. Song HK, Dougherty L. Dynamic MRI with projection reconstruction and KWIC processing for simultaneous high spatial and temporal resolution. Magn Reson Med 2004;52:815-824

36. Winkelmann S, Schaeffter T, Koehler T, Eggers H, Doessel O. An optimal radial profile order based on the golden ratio for time-resolved MRI. IEEE Trans Med Imaging 2007;26:68-76

37. Chan RW, Ramsay EA, Cheung EY, Plewes DB. The influence of radial undersampling schemes on compressed sensing reconstruction in breast MRI. Magn Reson Med 2012;67:363-377

38. Hedderich DM, Weiss K, Spiro JE, et al. Clinical evaluation of free-breathing contrast-enhanced T1w MRI of the Liver using pseudo golden angle radial k-space sampling. Rofo 2018;190:601-609

39. Kajita K, Goshima S, Noda Y, et al. Thin-slice free-breathing pseudo-golden-angle radial stack-of-stars with gating and tracking T1-weighted acquisition: an efficient gadoxetic acid-enhanced hepatobiliary-phase imaging alternative for patients with unstable breath holding. Magn Reson Med Sci 2019;18:4-11

40. Brodsky EK, Bultman EM, Johnson KM, et al. High-spatial and high-temporal resolution dynamic contrast-enhanced perfusion imaging of the liver with time-resolved three-dimensional radial MRI. Magn Reson Med 2014;71:934-941

41. Block KT, Frahm J. Spiral imaging: a critical appraisal. J Magn Reson Imaging 2005;21:657-668

42. Agrawal MD, Spincemaille P, Mennitt KW, et al. Improved hepatic arterial phase MRI with 3-second temporal resolution. J Magn Reson Imaging 2013;37:1129-1136

43. Xu B, Spincemaille P, Chen G, et al. Fast 3D contrast enhanced MRI of the liver using temporal resolution acceleration with constrained evolution reconstruction. Magn Reson Med 2013;69:370-381

44. Breuer FA, Blaimer M, Heidemann RM, Mueller MF, Griswold MA, Jakob PM. Controlled aliasing in parallel imaging results in higher acceleration (CAIPIRINHA) for multi-slice imaging. Magn Reson Med 2005;53:684-691

45. Breuer FA, Blaimer M, Mueller MF, et al. Controlled aliasing in volumetric parallel imaging (2D CAIPIRINHA). Magn Reson Med 2006;55:549-556

46. Kim BS, Lee KR, Goh MJ. New imaging strategies using a motion-resistant liver sequence in uncooperative patients. Biomed Res Int 2014;2014:142658

47. Wright KL, Harrell MW, Jesberger JA, et al. Clinical evaluation of CAIPIRINHA: comparison against a GRAPPA standard. J Magn Reson Imaging 2014;39:189-194

48. Michaely HJ, Morelli JN, Budjan J, et al. CAIPIRINHA-Dixon-TWIST (CDT)-volume-interpolated breath-hold examination (VIBE): a new technique for fast time-resolved dynamic 3-dimensional imaging of the abdomen with high spatial resolution. Invest Radiol 2013;48:590-597

49. Yu MH, Lee JM, Yoon JH, Kiefer B, Han JK, Choi BI. Clinical application of controlled aliasing in parallel imaging results in a higher acceleration (CAIPIRINHA)-volumetric interpolated breathhold (VIBE) sequence for gadoxetic acid-enhanced liver MR imaging. J Magn Reson Imaging 2013;38:1020-1026

50. Park YS, Lee CH, Kim IS, et al. Usefulness of controlled aliasing in parallel imaging results in higher acceleration in gadoxetic acid-enhanced liver magnetic resonance imaging to clarify the hepatic arterial phase. Invest Radiol 2014;49:183-188

51. Beck GM, De Becker J, Jones AC, von Falkenhausen M, Willinek WA, Gieseke J. Contrast-enhanced timing robust acquisition order with a preparation of the longitudinal signal component (CENTRA plus) for 3D contrast-enhanced abdominal imaging. J Magn Reson Imaging 2008;27:1461-1467

52. Eggers H, Bornert P. Chemical shift encoding-based water-fat separation methods. J Magn Reson Imaging 2014;40:251-268

53. Eggers H, Brendel B, Duijndam A, Herigault G. Dual-echo Dixon imaging with flexible choice of echo times. Magn Reson Med 2011;65:96-107

54. Berglund J, Ahlstrom H, Johansson L, Kullberg J. Two-point dixon method with flexible echo times. Magn Reson Med 2011;65:994-1004

55. Benkert T, Feng L, Sodickson DK, Chandarana H, Block KT. Free-breathing volumetric fat/water separation by combining radial sampling, compressed sensing, and parallel imaging. Magn Reson Med 2017;78:565-576

56. Pandharipande PV, Krinsky GA, Rusinek H, Lee VS. Perfusion imaging of the liver: current challenges and future goals. Radiology 2005;234:661-673

57. Thng CH, Koh TS, Collins DJ, Koh DM. Perfusion magnetic resonance imaging of the liver. World J Gastroenterol 2010;16:1598-1609

58. Sourbron S, Sommer WH, Reiser MF, Zech CJ. Combined quantification of liver perfusion and function with dynamic gadoxetic acid-enhanced MR imaging. Radiology 2012;263:874-883

59. Chen Y, Lee GR, Wright KL, et al. Free-breathing liver perfusion imaging using 3-dimensional through-time spiral

generalized autocalibrating partially parallel acquisition acceleration. Invest Radiol 2015;50:367-375

60. Chandarana H, Block TK, Ream J, et al. Estimating liver perfusion from free-breathing continuously acquired dynamic gadolinium-ethoxybenzyl-diethylenetriamine

pentaacetic acid-enhanced acquisition with compressed sensing reconstruction. Invest Radiol 2015;50:88-94

61. Hammernik K, Klatzer T, Kobler E, et al. Learning a variational network for reconstruction of accelerated MRI data. Magn Reson Med 2018;79:3055-3071